THE JOURNAL OF PHYSICAL CHEMISTRY B

ARTICLE

pubs.acs.org/JPCB

# Orientational Control over Nitrite Reductase on Modified Gold Electrode and Its Effects on the Interfacial Electron Transfer

Łukasz Krzemiński,[†] Samuel Cronin,[†] Lionel Ndamba,[‡] Gerard W. Canters,[‡] Thijs J. Aartsma,[‡] Stephen D. Evans,[§] and Lars J. C. Jeuken*[,†]

[†]Institute of Membrane and Systems Biology, University of Leeds, Woodhouse Lane, Leeds LS2 9JT, U.K.

[‡]Leiden Institute of Physics, Leiden University, P.O. Box 9504, 2300 RA, Leiden, The Netherlands

[§]School of Physics and Astronomy, University of Leeds, Woodhouse Lane, Leeds LS2 9JT, U.K.

**ABSTRACT:** Recently, studies have been reported in which fluorescently labeled redox proteins have been studied with a combination of spectroscopy and electrochemistry. In order to understand the effect of the dye on the protein−electrode interaction, voltammetry and surface analysis have been performed on protein films of dye-labeled and unlabeled forms of a cysteine-surface variant (L93C) and the wild type (wt) of the copper containing nitrite reductase (NiR) from *Alcaligenes faecalis* S6. The protein has been adsorbed onto gold electrodes modified with self-assembled monolayers (SAMs) made up of 6-mercaptohexanol (6-OH) and mixtures of various octanethiols. Electrochemical and surface-analytical techniques were utilized to explore the influence of the SAM composition on wt and L93C NiR enzyme activity and the orientation of the enzyme molecules with respect to the electrode/SAM. The unlabeled L93C NiR enzyme is only electroactive on mixed SAMs composed of positive 8-aminooctanethiol (8-$NH_2$) and 8-mercaptooctanol (8-OH). No enzymatic activity is observed on SAMs consisting of pure 6-OH, 8-OH, or pure 8-$NH_2$. Modification of L93C NiR with the ATTO 565 dye resulted in enzymatic activity on SAMs of 6-OH, but not on SAMs of 8-OH. Quartz crystal microbalance with dissipation measurements show that well-ordered and rigid protein films (single orientation of the protein) are formed when NiR is electroactive. By contrast, electrode−NiR combinations for which no electrochemical activity is observed still have NiR adsorbed on the surfaces, but a less-structured and water-rich film is formed. For the unlabeled L93C NiR, bilayer formation is observed, suggesting that the Cys93 residue is orientated away from the surface and able to form disulfide bridges to a second layer of L93C NiR. The results indicate that interfacial electron transfer is only possible if the negatively charged surface patch surrounding the electron-entry site of NiR is directed toward the electrode. This can be achieved either by introducing positive charges in the SAM or, when the SAM does not carry a charge, by labeling the enzyme with an ATTO 565 dye, which has some hydrophobic character, close to the electron entry site of the NiR.

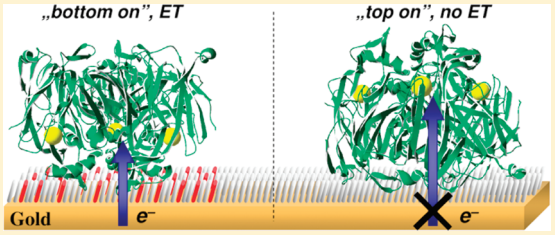


## INTRODUCTION

Nitrite reductase (NiR) from *Alcaligenes faecalis* S-6 is a copper-containing enzyme (Scheme 1), which takes part in microbial denitrification processes by catalyzing the one electron reduction of nitrite to nitric oxide: $NO_2^- + 2H^+ + e^- = NO + H_2O$.[1,2] The enzyme is a homotrimer, in which each subunit contains a type-1 Cu site and a type-2 Cu site.[3,4] The type-1 copper site, located close to the protein's surface, accepts electrons coming from the enzyme's natural donor, pseudoazurin, and acts as an electron relay by which electrons are transferred to the type-2 copper site, buried deep inside the enzyme.[3,5−10] The latter site, together with a water network around an aspartate and a histidine residue forms the catalytically active site of the enzyme.[3,4,11,12] Previously, it was shown that the catalytic cycle of NiR operates via a random sequential mechanism (RSM).[9,10,13] Spectroelectrochemistry studies,[13] in which a novel fluorescent technique[14,15] was used to examine the oxidation state of the type-1 Cu center during enzymatic turnover of NiR immobilized on modified gold, revealed that interfacial electron transfer (ET) between electrode and enzyme is heterogeneous and constitutes the rate-limiting step for catalysis by the immobilized NiR. Earlier spectroelectrochemical studies of fluorescently labeled azurin immoblized on SAM-covered gold electrodes had already provided proof for a considerable spread in ET rates and midpoint potential of the immobilized blue copper protein.[16] For a proper analysis of the enzyme's activity, it is essential, therefore, to understand the nature of the enzyme-electrode interactions. In particular, it is of interest to establish to what extent a covalently attached dye label may affect the rate of electron exchange between electrode and protein as well as the activity of the immobilized enzyme.

In general, for interfacial ET electronic coupling between the electrode and the enzyme's redox center is necessary. This coupling depends, among other things, on the protein's orientation on the electrode surface.[18−20] In turn, the orientation of enzymes physisorbed (i.e., noncovalently bound) on an electrode

**Received:** June 22, 2011
**Revised:** September 21, 2011
**Published:** September 22, 2011





dx.doi.org/10.1021/jp205852u | *J. Phys. Chem. B* 2011, 115, 12607–12614

**Scheme 1. Ribbon Diagram of L93C NiR Homotrimer from *Alcaligenes faecalis* S-6[a]**

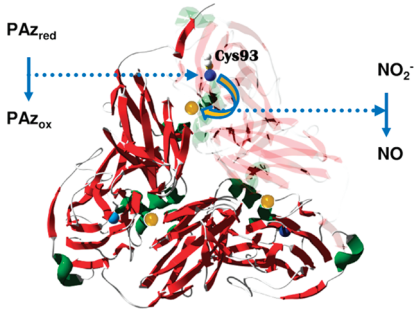


[a] Type-1 copper centers are rendered in blue, whereas type-2 copper sites have been colored in dark yellow. Surface-exposed cysteine residues (Cys93) are in close proximity to the type-1 copper (shown only on one monomer). Dotted arrows indicate the electron flow from reduced pseudoazurin ($PAz_{red}$) to nitrite ($NO_2^-$); see text for enzymatic reaction. The diagram was made with Swiss-PdbViewer v4.0.1 and POV-Ray v3.6 using adopted and modified NiR structural data[17].

depends on many factors, such as surface topology and charge of the electrode,[19−21] as well as pH, ionic strength, and viscosity of the buffer solution.[22−26] For over two decades, a common and very successful approach to control the properties of a gold interface has been to modify it with self-assembled monolayers (SAMs).[27,28] SAMs, particularly of alkanothiolates, are used conveniently to control biointerfacial chemistry. Here, SAMs are used to control the physicochemical properties of an electrode interface by manipulating the head-groups of the alkanethiol molecules. In this way the SAM−electrode surface can be made hydrophilic (−OH), hydrophobic ($-CH_3$), and/or charged ($-COO^-$ and $-NH_3^+$).

It is known that the interfacial ET rate across SAMs made from alkanethiols with more than six methylene groups decreases exponentially with the SAM thickness.[29,30] We, therefore, have employed six and eight carbon-atoms-long alkanethiols. Cyclic voltammetry (CV) was used to examine the electronic coupling between the modified gold electrode and physisorbed NiR molecules, and to test the enzyme's catalytic activity. The SAM was characterized by electrochemical impedance spectroscopy (EIS), while the mass and viscoelastic properties of the adsorbed biomolecules were examined with a quartz crystal microbalance with dissipation (QCM-D). The SAM layer composition and the surface charge of the enzyme appear crucial for sustaining interfacial ET and therefore enzymatic activity. The effect of NiR orientation on the rate of ET is discussed. Apart from the wild-type (wt) protein, we have used the L93C NiR variant. The surface-exposed Cys93 residue of the latter allows for the attachment of a dye molecule close to the type-1 copper site (ATTO-L93C NiR). Protein dimerization via disulfide bond formation was observed for immobilized L93C NiR molecules, but only when the latter are arranged with their Cys93 residues pointing into the solution.

## METHODS

**General.** Apart from protein labeling,[13] all experiments were performed in 20 mM 4-morpholine propane sulfonic acid (MOPS) (Sigma), pH 6.85, with 30 mM $Na_2SO_4$ (Sigma) as a supporting electrolyte. The buffer as well as all cleaning solutions were prepared using ultrapure Milli Q (Millipore) water of 18.2 MΩ, whereas thiol solutions were made up in isopropanol (HPLC grade, Fluka). All potentials are quoted versus a silver/silver chloride (Ag/AgCl) reference electrode (Radiometer, +199 mV with respect to the standard hydrogen electrode, SHE).

**Protein.** L93C NiR (from *Alcaligenes faecalis* S-6) was expressed and purified as described previously.[31] The copper content of the enzymes used for electrode experiments was 1.4 Cu/0.4 Zn per monomer of L93C NiR, as determined from atomic absorption spectroscopy. The Zn content in NiR was not taken into account in the analysis. The enzyme was labeled with ATTO 565 maleimide dye (ATTO-TEC GmbH) at the Cys93 position as previously described.[13] Briefly, prior to labeling, 200 μM L93C NiR (monomer) was reduced with 20× molar excess of the reducing agent tris(2-carboxyethyl)phosphine (TCEP, Sigma), in order to break disulfide bonds that have formed between L93C NiR trimers. We note that this step was required for reproducible labeling, indicating that disulfide bridges are formed between L93C NiR trimers during storage. After size exclusion chromatography (Centri-Spin 10 columns, Princeton Separations) in order to remove TCEP, a 3-fold excess of ATTO 565 maleimide over 100 μM protein monomer was used to label L93C NiR, after which free label was removed by gel filtration. The labeling reaction was performed in *N*-(2-hydroxyethyl)piperazine-*N*′-ethanesulfonic acid (HEPES) buffer at pH 7.3 (Sigma).

**Electrode Modification.** All experiments were carried out with template stripped gold (TSG) working electrodes.[32,33] SAMs were prepared by incubating the TSG slide with 1.5 mM of 6-mercapto-hexanol (6-OH, Sigma), 8-mercaptooctanol (8-OH, Sigma), 8-amino-1-octanethiol (8-$NH_2$, NBS Biologicals), 1-octanethiol (7-$CH_3$, Sigma), or 8-mercaptooctanoic acid (7-COOH, Sigma) for 5 h at 21 °C in isopropanol. For the mixed thiols, the total thiol concentration in the isopropanol solution was kept at 1.5 mM. Subsequently, the excess thiol was washed away with isopropanol and methanol; the electrodes were then dried in a stream of $N_2$ and incubated with 3 μM (monomer concentration) of NiR for 20 min. Directly after this, the enzyme-modified electrode was rinsed three times with water/buffer and used in the electrochemistry experiments.

**EIS and CV.** An electrochemical cell of all-glass construction was used, with the main compartment housing the gold working electrode, in which the TSG surfaces were embedded in a PTFE holder with a rubber O-ring, ($A$ = 0.21 $cm^2$), a platinum wire counter electrode and a saturated silver/silver chloride electrode (Ag/AgCl). The cell was enclosed in a Faraday cage to minimize electrical noise and purged with Argon to remove oxygen. EIS spectra were recorded on each SAM electrode prior to the addition of protein, using an Autolab electrochemical analyzer (Eco-chemie, Utrecht, The Netherlands) equipped with a PGSTAT30 potentiostat, SCANGEN module and FRA2 frequency analyzer. EIS results were fitted by home-built software that uses a Levenberg−Marquardt procedure, and the errors in the parameters were analyzed using a Monte Carlo bootstrap method.[32,33] Analogue CVs were recorded (same potentiostat, scan rate 10 mV/s) on enzyme-modified electrodes prior to and after the addition of the substrate (40 mM nitrite). The potential window used was from +300 mV to −400/500 mV vs Ag/AgCl. The electroactive coverage of the enzyme on 6-OH SAM electrodes covered with labeled NiRs (ATTO-L93C NiR) was determined from noncatalytic voltammograms recorded by using SOAS software, freely available from Dr. C. Léger.[34]

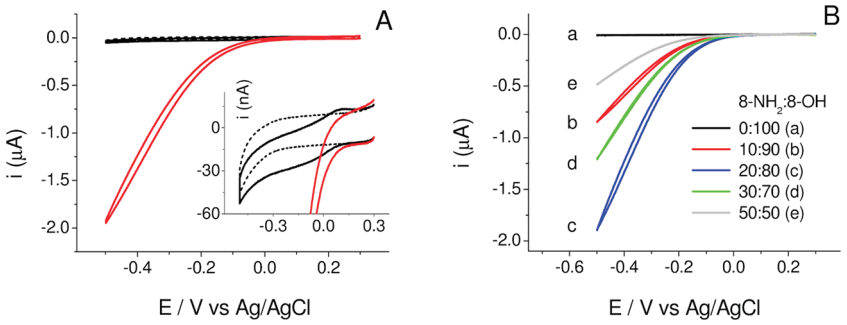


**Figure 1.** (A) CVs from L93C NiR adsorbed on 20%:80% 8-$NH_2$:8-OH SAM electrode, recorded in the absence (solid black line) and presence (red line) of 40 mM nitrite. The inset (zoom in) shows the enzyme peaks in the absence of nitrite (solid black line) compared to a blank CV of the mixed SAM only (dashed black line). (B) Series of baseline-subtracted CVs showing L93C NiR activity on mixed SAM electrodes of different 8-$NH_2$:8-OH ratios. All CVs were recorded at pH 6.85 and 10 mV/s scan rate.

**QCM-D.** QCM-D experiments were conducted on a Q-Sense E4 (Q-Sense AB, Gothenburg, Sweden). Experiments were performed using gold sensor crystals at 22 °C, with the flow rate held at 70 $\mu$L/min. QCM-D sensors were cleaned by incubating them with MilliQ water (30 min), 0.4% sodium dodecyl sulfate (SDS) detergent (20 min), and again Milli-Q water (20 min). After that, gold-covered crystals were treated for 20 min with UV/ozone (UV/ozone cleaning system, low-pressure quartz−mercury vapor lamp emitting 254 and 185 nm UV, UVOCS, Montgomeryville) followed by 40 min in ethanol to reduce the gold.[35] Immediately after, the crystals were transferred into the thiol solutions, as mentioned above. On graphs, changes in the dissipation ($\Delta D$), and frequency, ($\Delta f$) of the seventh overtone are presented only, while we also recorded 3rd, 5th, 9th, 11th, and 13th overtones. The cumulative data were used during the modeling of viscoelastic properties of the adsorbed proteins. The modeling was performed using QTools 2 Qsense software under the assumptions of the Kelvin−Voight model[36,37] and a hydrodynamic protein layer density[38−41] of 1200 kg/m$^3$. The viscosity and density of the buffer used were assumed to be 0.001 kg/ms and 1000 kg/m$^3$, respectively.

## RESULTS AND DISCUSSION

**CV and EIS on 8-X SAM Electrodes (unlabeled L93C NiR).** The unlabeled L93C enzyme was found to be active only on mixed SAMs composed of 8-OH and 8-$NH_2$. The enzyme electrodes with SAMs of pure 8-OH, 8-$NH_2$, 7-$CH_3$, and 7-COOH, as well as mixtures of 8-OH/7-COOH and 8-OH/7-$CH_3$ did not show catalytic waves after $NO_2^-$ addition, despite the fact that the protein is able to physisorb on all these electrodes (*vide infra*). This indicates that the L93C NiR orientation on the surface is key for its activity, in line with previous studies.[7,8] Figure 1A (inset, black solid line) shows a typical voltammetric response of L93C NiR adsorbed on a 20%:80% 8-$NH_2$:8-OH SAM electrode, recorded in the absence of nitrite. Besides the redox peaks due to the L93C NiR oxidation and reduction, a slight catalytic wave can be observed, which we suggest is due to a relatively slow reduction of oxygen to hydrogen peroxide by the enzyme, as previously observed.[6] In the presence of nitrite (Figure 1A, red line) a strong catalytic current ($i_{cat}$) is observed when the electrode potential is taken below 0 V vs Ag/AgCl. The slope of this current−potential plot has previously been reported by us[9,10,13] and others[18,42] to reflect the heterogeneity in the rates of ET to the protein molecules on the electrode surface.

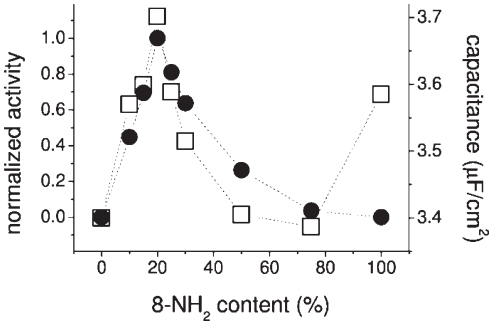


**Figure 2.** Electric double layer capacitance changes (open squares) from mixed SAM electrodes with increasing 8-$NH_2$:8-OH ratio. The enzymatic activity changes (filled circles) of L93C NiR adsorbed on corresponding electrodes is also shown.

Variation of the ratio of the SAM components (8-$NH_2$ and 8-OH) revealed that the enzyme's activity depends strongly on the 8-$NH_2$ content in the SAM. Figure 1B and Figure 2 (filled circles) show an increase in $i_{cat}$ when the 8-$NH_2$ content is increased from 0% to 20%. This is followed by a decrease at higher concentrations of 8-$NH_2$. The maximum $i_{cat}$ occurs at a 8-$NH_2$:8-OH ratio of 20%:80%. Interestingly, a similar dependence was found for the electric double layer capacitance ($C_{dl}$) (measured before protein addition). Figure 2 shows that the activity profile of the L93C NiR (filled circles) follows the $C_{dl}$ change (open squares), apart from the data point corresponding to a pure 8-$NH_2$ SAM. We also note that the lowest $C_{dl}$ is observed for SAMs formed with the hydrophobic 7-$CH_3$. SAMs of 7-COOH/8-OH (negative surface) have $C_{dl}$ similar to that of the 8-$NH_2$:8-OH SAMs, while the highest $C_{dl}$ are recorded for pure 7-COOH and 6-OH monolayers (Table 1).

As the double layer capacitance depends on the separation between electrolyte ions and the gold surface, these $C_{dl}$ variations are generally attributed to changes in SAM layer thickness and/or structure.[43,44] According to this, SAMs composed of shorter length thiols (thinner monolayers) have a higher capacitance (6-OH vs 8-OH). The capacitance depends further on the hydrophilicity and the fluidity of the SAMs in the following order: $SH-(CH_2)_n-CH_3 < SH-(CH_2)_n-OH < SH-(CH_2)_n-NH_3^+ = SH-(CH_2)_n-COO^-$.[43,44] Hydrophilic SAM layers interact more strongly with water and the electrolyte ions and are penetrated to a larger extend by the electrolyte. This increases the dielectric constant of the SAM layer and causes the capacitance to increase.[43,44]

**Table 1. Electric Double Layer Capacitance Values ($C_{dl}$) Measured for SAM-Modified Gold Electrodes**

| SAM electrode | $C_{dl}$ ($\mu$F/cm$^2$) |
|---|---|
| 8-OH | 3.40 |
| 6-OH | 5.57 |
| 7-COOH | 6.13 |
| 7-$CH_3$ | 1.54 |
| 20%:80% 7-COOH:8-OH | 4.13 |
| 10%:90% 7-COOH:8-OH | 3.71 |

It explains why an increase in $C_{dl}$ is observed as 8-$NH_2$ is titrated into the 8-OH SAM layer, but it does not explain the drop in capacitance at coverages above 20% 8-$NH_2$ (Figure 2, open squares). The later observation may be explained by considering the depolarization effect in SAMs.[45−48]

Depolarization is a consequence of the fact that the electron cloud of every molecule within the SAM is polarized by the electric field that is the superposition of the fields generated by all other molecules in the SAM.[45−48] In homogeneous SAM layers (e.g., pure 8-OH or 8-$NH_2$), the field of each dipole induces oppositely oriented dipoles in all neighbors. This results in a net depolarization in SAMs of dipolar molecules. In mixed SAMs, however, the opposite effect is expected. The antiparallel orientation of neighboring dipoles within the SAM leads to mutual polarization giving rise to increased dipole moments.[45−48] This creates a higher dielectric, therefore increasing its capacitance (Figure 2, open squares). Significant charge rearrangements within mixed SAMs will then depend on thiol-components polarity and their ratio. The pure 8-OH and 8-$NH_2$ SAMs will therefore exhibit a weaker overall polarization than a mixed SAM. The maximum polarization apparently occurs at a 20%:80% ratio of 8-$NH_2$ to 8-OH.

The enzyme's activity parallels the polarization of the SAM (Figure 2). Maximum activity is observed at a 20%:80% ratio of 8-$NH_2$ to 8-OH. This can be understood by considering the surface charge of the L93C NiR molecule. The negatively charged patch around the type-1 Cu site[49] is the recognition and docking site for a complementary, positively charged surface patch of the physiological ET partner of NiR, pseudoazurin.[5,8,49,50] It may be expected, therefore, that L93C NiR will be more active on a more positively charged SAM electrode (higher 8-$NH_2$ content). That the highest activity is observed with the 20%:80% 8-$NH_2$:8-OH SAM electrode is compatible with the idea (*vide supra*) that, for this 8-$NH_2$:8-OH ratio, the SAM presents the highest density of positive charge toward the NiR molecules, thus enabling the maximum Coulomb-mediated absorption of L93C NiRs on the electrode.

**CV and EIS on a 6-OH SAM Electrode (Unlabeled and Labeled L93C NiR).** Labeling the enzyme with the ATTO 565 dye (ATTO-L93C NiR) results in the enzymatic activity on gold modified with pure 6-OH. Figure 3 (solid red line) illustrates a current−potential dependence similar to that presented in Figure 1A, indicating nitrite turnover by the enzyme, whereas no NiR activity is observed when unlabeled L93C NiR is used (Figure 3, dashed red line). At the same time, we note that both ATTO-L93C NiR and L93C NiRs are shown to bind to the 6-OH SAM electrode (QCM-D section below), which, again, suggests that the enzyme activity on the electrode is controlled by the orientation of the NiR on the electrode. ATTO-L93C NiR on a 6-OH SAM exhibits approximately half of the activity of the previously discussed L93C NiR on a mixed SAM electrode

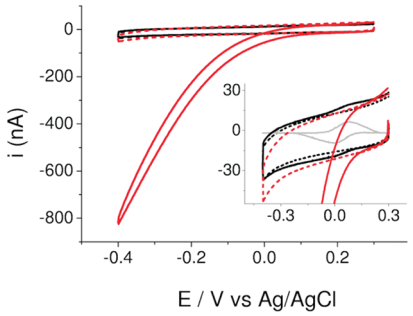


**Figure 3.** CVs from ATTO-L93C NiR (solid red line) and L93C NiR (dashed red line) adsorbed at 6-OH SAM electrode, recorded in the presence of 40 mM nitrite. The inset (zoom in) shows the enzyme's redox peaks of ATTO-L93C NiR on the electrode in the absence of nitrite (solid black line) compared to the blank CV of 6-OH SAM only (dashed black line). Gray stands for the baseline-subtracted protein signal. All CVs were recorded at pH 6.85 and 10 mV/s scan rate.

(20%:80% 8-$NH_2$:8-OH). We think that this is because the latter electrode is positively charged, further optimizing the orientation of the enzyme for interfacial ET.

In the absence of nitrite and with extended purging with argon, we were able to determine the reduction and oxidation peaks of ATTO-L93C NiR, at 0 V ± 10 mV and 78 mV ± 10 mV vs Ag/AgCl, respectively (Figure 3 inset), in good agreement with the literature.[1,9,51,52] Using the area underneath the redox peaks, an electroactive coverage of 1.66−1.85 pmol/cm$^2$ is determined, which constitutes only 20−23% of all enzymes adsorbed on the electrode (see QCM-D section below). Elsewhere,[13] we have reported that all of the ATTO-L93C NiR subunits (homotrimer) are catalytically active with one monomer experiencing faster electron exchange with the electrode than the other two monomers. Therefore, we attribute the difference between the coverage determined from CV and from QCM-D to the fact that two monomers within the trimer exhibit slow electron-transfer kinetics and do not contribute to the magnitude of the redox-signals in the CV at 10 mV/s (Figure 3 inset, solid black line). Instead they produce a much broader, undetectable redox signal.

Importantly, labeling of the protein does not result in activity on any of the other SAM electrodes, including the 8-OH SAM. This is especially intriguing if we compare 6-OH and 8-OH thiols, which differ in length by only two methylene groups. The 40% increase in capacitance of 6-OH SAM compared to 8-OH SAM (Table 1) is approximately 2 times higher than expected on the basis of the difference in chain length. This reflects the less crystalline nature of a 6-OH SAM over an 8-OH SAM.[44] ATTO-L93C NiR is labeled with a zwitterionic ATTO 565 fluorophore that is covalently linked to Cys93 located close to the type-1 Cu site (0.7 nm as estimated from NiR crystallographic data,[17] Scheme 1). ATTO 565 contains a carboxylic-acid group and a positive cyclic amine, while the overall conjugated ring structure also has a hydrophobic character. We speculate that the ATTO 565 interacts more strongly with the more-fluid 6-OH than the 8-OH SAM and helps to orientate the NiR on the 6-OH electrodes. It is possible that the dye is able to intercalate into the 6-OH SAM, while the more crystalline 8-OH SAM prohibits this type of interaction. The latter hypothesis would provide a rationalization for the unexpected difference in activity of ATTO-L93C NiR on the 6-OH and 8-OH SAMs.

**QCM-D.** The effect of the titration of 8-$NH_2$ into the 8-OH monolayer and the effect of enzyme labeling (6-OH SAM) on the

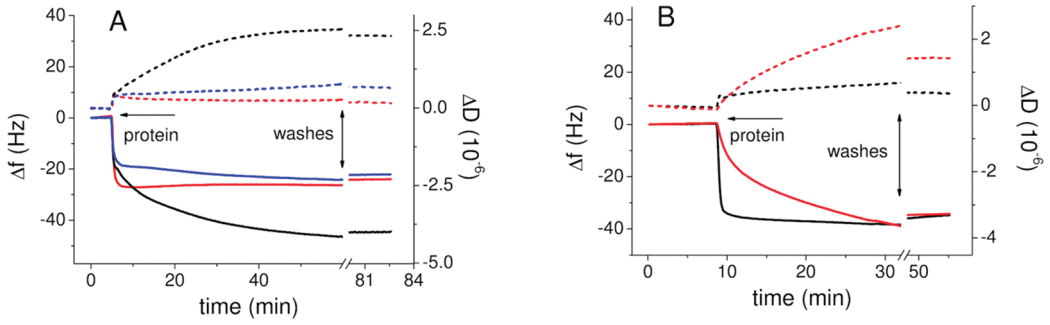


**Figure 4.** (A) Frequency ($\Delta f$, solid lines) and dissipation changes ($\Delta D$, dashed lines) from ATTO-L93C NiR (red), L93C NiR (black), and wt NiR (blue) during adsorption on 6-OH SAM electrodes. (B) The $\Delta f$ (solid lines) and $\Delta D$ (dashed lines) changes from L93C NiR adsorption on 20%:80% 8-$NH_2$:8-OH (black) and pure 8-OH (red) SAM electrodes. In all cases NiR concentration (monomer) was 3 $\mu$M, pH 6.85.

**Table 2. Viscoelastic Properties Together with Mass Coverage Calculations of Different NiR Variants Adsorbed on SAM Electrodes**[a]

| NiR variant | | L93C NiR | | | | ATTO-L93C NiR | wt NiR |
|---|---|---|---|---|---|---|---|
| SAM | | 6-OH | | 8-OH | 20%:80% 8-$NH_2$:8-OH | 6-OH | 6-OH |
| Voight values | | layer 1 | layer 2 | | | | |
| | viscosity (kg/ms) | 0.006 | 0.003 | - | 0.008 | 0.009 | 0.006 |
| | shear (MPa) | 2 | 0.4 | - | 7 | 8 | 2 |
| | thickness (nm) | 3.5 | 3.9 | - | 5.3 | 3.6 | 3.5 |
| Sauerbrey values | mass (ng/cm$^2$) | 800 | | 620 | 620 | 430 | 400 |
| | coverage (%) | 140 | | 110 | 110 | 80 | 75 |

[a] The analysis was performed on Figure 4, $\Delta f$ and $\Delta D$ data obtained after the final protein wash with buffer. The underlined values were fixed during Voight modeling.

NiR adsorption profiles was monitored with QCM-D. The data indicate two kinetic regimes for protein adsorption (Figure 4). For the electrode−protein combinations that exhibit enzymatic activity (i.e., L93C NiR on 20%:80% 8-$NH_2$:8-OH and ATTO-L93C NiR on a pure 6-OH SAM) fast adsorption is observed with low values of dissipation, similar to the immobilization of electroactive azurin on SAM-modified gold.[53] For electrodes that did not show any electrochemical activity of NiR (i.e., L93C NiR on a pure 6-OH or 8-OH SAM), a significantly slower adsorption is observed. The higher dissipations of protein films of electroinactive NiR suggest the protein orientation is dynamic and the presence of hydrodynamically trapped water.[26,37,38,40]

To estimate the enzyme's homotrimer coverage on the electrodes (after washing the electrode with buffer) a molecular weight of 140 kDa was used to include 25% mass water, which is an average water content for proteins.[40,54] From the NiR crystal structure[17] we calculate that a full homotrimer monolayer corresponds to ~4 pmol/cm$^2$, independent of its orientation. The Sauerbrey's equation[55−57] was used to calculate the adsorbed mass and the Voigt model[36,37] to describe the viscoelastic properties of the protein film. The extracted values are summarized in Table 2. Moreover, in order to better understand the protein−surface interactions we have analyzed $\Delta D - \Delta f$ plots (Figure 5), the slope of which ($K = |\delta\Delta D/\delta\Delta f|$) is diagnostic of changes in orientation during the protein adsorption. In literature, small values of $K$ are ascribed to rigid layers, whereas a high values point to a soft and water-rich layer.[38,40,41]

**6-OH SAM Electrode (ATTO-L93C NiR, L93C NiR, and wt NiR).** Figure 5A (open circles) displays two phases with significantly different slopes ($K_2 > K_1$), indicating that, when L93C NiR adsorbs to 6-OH SAM electrodes, two separate kinetic phases occur with different viscoelastic properties.[26,40,41] Interestingly, the initial phase of the adsorption ($K_1$) is the same as that of ATTO-L93C NiR (Figure 5A, open squares) and wt NiR (Figure 5A, open triangles). However, once the labeled enzyme reaches about 80% of the maximal calculated surface coverage (Table 2), no further adsorption is observed (Figure 4A, red lines), while for the L93C NiR a second phase follows (Figure 4A, black lines). We conclude that ATTO-L93C NiR looses more of its trapped water upon binding to the surface (Figure 5A, arrow) to give a rigid monolayer (Table 2). The fact that ET to the enzyme is possible on the millisecond-to-second time scale and that the film thickness amounts to 3.6 nm suggest that the enzyme molecules bind in a bottom-on configuration with type-1 Cu sites facing the electrode surface. The layer is 15% thinner than the theoretical value of 4.4 nm (Table 2), which has also been observed for other protein films and has been ascribed to proteins spreading out upon adsorption.[40]

By contrast, L93C NiR continues to bind to the surface after the first monolayer is formed (coverage of 140%, Table 2). According to Figure 5A this second layer is much more dynamic when compared to the underlying, stiffer NiR film ($K_2 > K_1$). This is also reflected in the viscoelastic properties of the whole film. Assuming the parameters of the first layer to be similar to wt NiR ($K_1$), the second protein layer exhibits a highly reduced viscosity and shear modulus at similar mass (Table 2), indicative of a soft and water-rich protein film that will dissipate the energy more efficiently.[38,40,41] Thus, the observed $\Delta D$ value of the film is significantly higher than in the case of the previously discussed, rigid film composed of labeled proteins (Figure 4A). This is

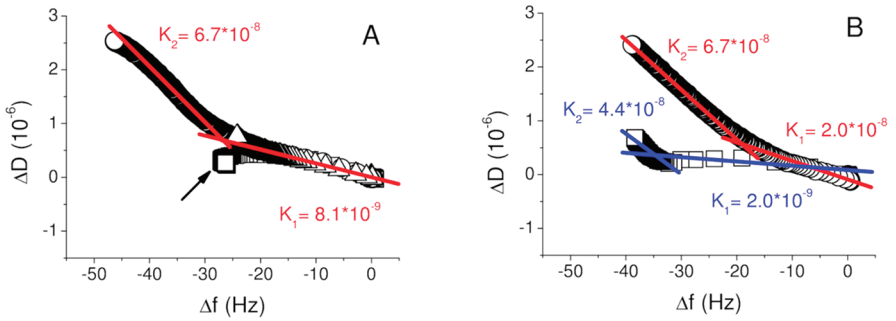


**Figure 5.** The $\Delta D/\Delta f$ representation of Figure 4 data obtained before the protein wash with buffer. (A) Open squares represent ATTO-L93C NiR (red fit, $K_1$), open circles stand for L93C NiR (red fits, $K_1$ and $K_2$) and open triangles represent wt NiR (red fit, $K_1$) adsorption profiles on 6-OH SAM electrodes. (B) Open squares illustrate L93C NiR adsorption on 20%:80% 8$NH_2$:8-OH SAM (blue fits, $K_1$ and $K_2$), while open circles show L93C NiR adsorbing to pure 8-OH SAM electrode (red fits, $K_1$ and $K_2$).

consistent with other studies[26,40,58,59] showing that energy dissipation is generally higher in the second layer, which is attributed to more dynamic properties of water that is trapped between the two protein layers as well as to high energy losses in the more flexible and more weakly bound protein molecules.

The second protein layer and the lack of electroactivity from L93C NiR on 6-OH SAM electrodes (electrochemistry section above) can be explained if we consider that the enzyme used in this study is a NiR variant with a surface-exposed cysteine residue Cys93 labeled. Therefore, the unlabeled enzymes could adsorb in two layers with the first layer in a top-on orientation, in which the type-1 copper sites face away from the electrode. Enzyme molecules can then build up a second layer by means of disulfide bond formation (Scheme 2C). Cysteine bridges cannot form in the case of the ATTO-L93C NiR, as the Cys93 residues are blocked by the dye (~30% labeling efficiency) and by the electrode, consistent with the previously proposed bottom-on orientation of these molecules (Scheme 2A).

Finally, for wt NiR on 6-OH only a single protein layer is formed and no electroactivity is observed. Again, this is consistent with a top-on orientation. The absence of the Cys93 residues precludes the formation of the second layer.

**Pure 8-OH and 20%:80% 8-$NH_2$:8-OH SAM Electrode (L93C NiR).** Unlike the binding data obtained for different NiR variants on a 6-OH SAM electrode (initial phase in Figure 5A), the data obtained for 20%:80% 8-$NH_2$:8-OH and pure 8-OH electrodes have little in common (Figure 5B). The $\Delta D - \Delta f$ representation of L93C NiR adsorbed on 20%:80% 8-$NH_2$:8-OH SAM (Figure 5B, open squares) indicates the formation of a compact enzyme film ($K_1$) followed by a second phase exhibiting minor and weak protein adsorption ($K_2$). These weakly adsorbed L93C NiR molecules are easily washed away with buffer, as can be observed from the final changes in $\Delta D$ and $\Delta f$ signals (Figure 4B, black lines after 40 min).

The molecular coverage (110%) of L93C NiR and the viscoelastic properties observed for this mixed SAM electrode, when compared to ATTO-L93C NiR on a 6-OH SAM (Table 2), suggest the occurrence of more than one enzyme layer. An alternative explanation could be that not all NiR molecules are bottom-on oriented as in the case of ATTO-L93C NiR on 6-OH SAM. Instead, part of the enzyme monolayer might have a side-on configuration that will result in a thicker film (Table 2) and a different packing of L93C NiR molecules on the surface. The analysis of the data obtained for L93C NiR adsorbed on a pure 8-OH SAM reveals a pattern similar to that for the L93C enzyme on a 6-OH SAM electrode. Figure 5B (red lines) shows two kinetic phases for the absorption of the protein. However, the high dissipation values correspond to the formation of a non-ordered and flexible protein film. Unlike other cases, the protein molecules seem to undergo prolonged reorientations on the surface before they finally stabilize. Meanwhile, new L93C NiR molecules bind to them through the surface exposed Cys93 residues ($K_2$), similar to L93C NiR on a 6-OH SAM electrode ($K_2$ in Figure 5A). Again, the lack of enzymatic activity (*vide supra*) indicates that L93C NiR molecules in the first layer (in direct contact with the electrode) are adsorbed in a top-on fashion in which the type-1 Cu sites face away from the electrode.

**Scheme 2. Schematic Representation of ATTO-L93C NiR Orientation on 6-OH SAM (A), L93C NiR on 20%:80% 8$NH_2$:8-OH SAM (B), and 6-OH SAM (C) electrodes**[a]

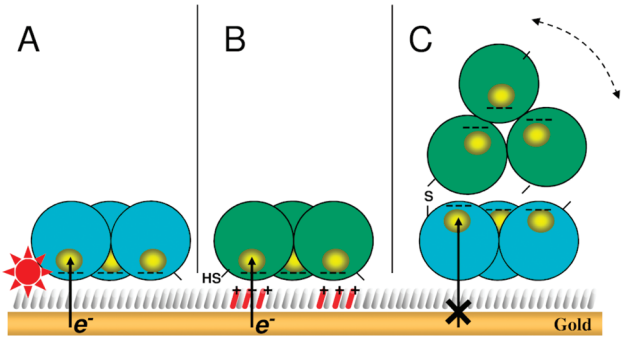


[a] A and B illustrate the electroactive, bottom-on, NiR orientation on the electrodes, for which direct ET occurs from modified gold to type-1 copper centers within the enzyme molecules. C represents electroinactive, top-on, L93C NiR orientation on SAM electrodes, for which direct ET cannot occur because of a lack of electrical coupling between gold and the redox centers of NiR (type-1 copper sites). The position of Cys93 is shown (−SH, −). The mobility of the disulfide-coupled L93C NiR molecules is symbolized by a dashed arrow. Red features in A and B stand for ATTO 565 dye and positively charged 8-$NH_2$ alkanethiols, respectively.

## CONCLUSIONS

We have shown how the orientation of NiR molecules with respect to the electrode surface affects the enzyme electroactivity. First, activity of unlabeled L93C NiR is only found at a gold electrode modified with mixtures of 8-$NH_2$ and 8-OH SAM.

The presence of 8-$NH_2$ introduces positive charge in the SAM-surface. The enzyme binds to the positively charged surface via its negative patch, which surrounds the entry point for electrons on their way to the type-1 copper center. This, apparently, provides the best electronic coupling between type-1 copper site and the gold resulting in direct ET and thus enzymatic activity upon substrate addition. Second, L93C NiR modification with a ATTO 565 dye (ATTO-L93C NiR) results in activity on 6-OH modified electrodes, but not on 8-OH modified surfaces. We suggest that the reason for this is the interaction between the small organic dye molecule and the 6-OH SAM layer that may orient the redox face of the enzyme toward the electrode surface. QCM-D data attest to the formation of well-ordered, rigid protein films for L93C NiR on a 20%:80% 8-$NH_2$:8-OH SAM and ATTO-L93C NiR on a 6-OH SAM. The data are consistent with NiR adopting a bottom-on orientation on the surface by which the type-1 Cu sites face the gold electrode, although some may also orient in a side-on fashion. Overall, the film consists of proteins in a single orientation (Scheme 2A and 2B). By contrast, a bilayer of L93C NiR is found for electrodes on which no electrochemical activity of NiR is observed. In this latter case, L93C NiRs form a more dynamic and water-rich film. The enzymes close to the electrode are more rigid than the enzymes in the second protein layer. The proteins in the first layer adopt a top-on configuration, in which the type-1 copper sites are positioned away from the electrodes together with the surface-exposed Cys93 residues. This impedes ET between electrode and enzyme and allows other L93C NiR molecules to bind via disulfide bond formation (Scheme 2C).

## AUTHOR INFORMATION

### Corresponding Author

*E-mail: L.J.C.Jeuken@leeds.ac.uk.

## ACKNOWLEDGMENT

This work was supported by the European Community (FP6) through the Marie Curie Research Training Network "EdRox" (Contract No. MRTN-CT-2006-035649).

## REFERENCES

(1) Adman, E. T.; Murphy, M. E. P. *Handbook of Metalloproteins*; Messerschmidt, A., Huber, R., Wieghardt, K., Poulos, T., Eds; John Wiley & Sons, Ltd.: Chichester, U.K., 2001; 1381−1390.

(2) Wasser, I. M.; de Vries, S.; Moenne-Loccoz, P.; Schroder, I.; Karlin, K. D. *Chem. Rev.* **2002**, *102*, 1201–1234.

(3) Kukimoto, M.; Nishiyama, M.; Murphy, M. E.; Turley, S.; Adman, E. T.; Horinouchi, S.; Beppu, T. *Biochemistry* **1994**, *33*, 5246–5252.

(4) Libby, E.; Averill, B. A. *Biochem. Biophys. Res. Commun.* **1992**, *187*, 1529–1535.

(5) Kukimoto, M.; Nishiyama, M.; Tanokura, M.; Adman, E. T.; Horinouchi, S. *J. Biol. Chem.* **1996**, *271*, 13680–13683.

(6) Kakutani, T.; Watanabe, H.; Arima, K.; Beppu, T. *J. Biochem.* **1981**, *89*, 463–472.

(7) Astier, Y.; Bond, A. M.; Wijma, H. J.; Canters, G. W.; Hill, H. A. O.; Davis, J. J. *Electroanalysis* **2004**, *16*, 1155–1165.

(8) Astier, Y.; Canters, G. W.; Davis, J. J.; Hill, H., A.; Verbeet, M. P.; Wijma, H. J. *ChemPhysChem* **2005**, *6*, 1114–1120.

(9) Wijma, H. J.; Jeuken, L. J.; Verbeet, M. P.; Armstrong, F. A.; Canters, G. W. *J. Am. Chem. Soc.* **2007**, *129*, 8557–8565.

(10) Wijma, H. J.; Jeuken, L. J.; Verbeet, M. P.; Armstrong, F. A.; Canters, G. W. *J. Biol. Chem.* **2006**, *281*, 16340–16346.

(11) Boulanger, M. J.; Kukimoto, M.; Nishiyama, M.; Horinouchi, S.; Murphy, M. E. *J. Biol. Chem.* **2000**, *275*, 23957–23964.

(12) Zhao, Y.; Lukoyanov, D. A.; Toropov, Y. V.; Wu, K.; Shapleigh, J. P.; Scholes, C. P. *Biochemistry* **2002**, *41*, 7464–7474.

(13) Krzemiński, Ł.; Ndamba, L.; Canters, G. W.; Aartsma, T. J.; Evans, S. D.; Jeuken, L. J. C. *J. Am. Chem. Soc.* **2011**, *133*, 15085–15093.

(14) Schmauder, R.; Alagaratnam, S.; Chan, C.; Schmidt, T.; Canters, G. W.; Aartsma, T. J. *J. Biol. Inorg. Chem.* **2005**, *10*, 683–687.

(15) Kuznetsova, S.; Zauner, G.; Schmauder, R.; Mayboroda, O. A.; Deelder, A. M.; Aartsma, T. J.; Canters, G. W. *Anal. Biochem.* **2006**, *350*, 52–60.

(16) Salverda, J. M.; Patil, A. V.; Mizzon, G.; Kuznetsova, S.; Zauner, G.; Akkilic, N.; Canters, G. W.; Davis, J. J.; Heering, H. A.; Aartsma, T. *J. Angew. Chem. Int. Ed.* **2010**, *49*, 5776–5779.

(17) Murphy, M. E.; Turley, S.; Adman, E. T. *J. Biol. Chem.* **1997**, *272*, 28455–28460.

(18) Leger, C.; Bertrand, P. *Chem. Rev.* **2008**, *108*, 2379–2438.

(19) Kasmi, A. E.; Wallace, J. M.; Bowden, E. F.; Binet, S. B.; Linderman, R. J. *J. Am. Chem. Soc.* **1998**, *120*, 225–226.

(20) Chen, X.; Ferrigno, R.; Yang, J.; Whitesides, G. M. *Langmuir* **2002**, *18*, 7009–7015.

(21) Leopold, M. C.; Bowden, E. F. *Langmuir* **2002**, *18*, 2239–2245.

(22) Groot, M. T.; Merkx, M.; Koper, M. T. M. *Langmuir* **2007**, *23*, 3832–3839.

(23) Yue, H.; Waldeck, D. H. *Curr. Opin. Solid State Mater. Sci.* **2005**, *9*, 28–36.

(24) Millo, M.; Bonifacio, A.; Ranieri, A.; Borsari, M.; Gooijer, C.; Zwan, G. *Langmuir* **2007**, *23*, 9898–9904.

(25) Jeuken, L. J. *Biochim. Biophys. Acta* **2003**, *1604*, 67–76.

(26) Höök, F.; Rodahl, M.; Kasemo, B.; Brzezinski, P. *Proc. Natl. Acad. Sci. U.S.A.* **1998**, *95*, 12271–12276.

(27) Nuzzo, R. G.; Allara, D. L. *J. Am. Chem. Soc.* **1983**, *105*, 4481–4483.

(28) Arya, S. K.; Solankia, P. S.; Dattab, M.; Malhotra, B. D. *Biosens. Bioelectron.* **2009**, *24*, 2810–2817.

(29) Chi, Q.; Zhang, J.; Arslan, T.; Borg, L.; Pedersen, G. W.; Christensen, H. E. M.; Nazmudtinov, R. R.; Ulstrup, J. *J. Phys. Chem. B* **2010**, *114*, 5617–5624.

(30) Smalley, J. F.; Finklea, H. O.; Chidsey, C. E. D.; Linford, M. R.; Creager, S. E.; Ferraris, J. P.; Chalfant, K.; Zawodzinsk, T.; Feldberg, O. S. W.; Newton, M. D. *J. Am. Chem. Soc.* **2004**, *125*, 2004–2013.

(31) Wijma, H. J.; Boulanger, M. J.; Molon, A.; Fittipaldi, M.; Huber, M.; Murphy, M. E.; Verbeet, M. P.; Canters, G. W. *Biochemistry* **2003**, *42*, 4075–4083.

(32) Jeuken, L. J. C.; Daskalakis, N. N.; Han, X.; Sheikh, K.; Erbe, A.; Bushby, R. J.; Evans, S. D. *Sens. Actuators B* **2007**, *124*, 501–509.

(33) Jeuken, L. J. C.; Connell, S. D.; Henderson, P.; Gennis, R. B.; Evans, S. D.; Bushby, R. J. *J. Am. Chem. Soc.* **2006**, *128*, 1711–1716.

(34) Fourmonda, V.; Hokec, K.; Heeringd, H. A.; Bafferet, C. L. F.; Bertranda, P.; Leger, C. *Bioelectrochemistry* **2009**, *76*, 141–147.

(35) Kendall, J. K. R.; Johnson, B. R. G.; Symonds, P. H.; Imperato, G.; Bushby, R. J.; Gwyer, J. D.; Berkel, C.; Evans, S. D.; Jeuken, L. J. C. *ChemPhysChem* **2010**, *11*, 2191–2198.

(36) Liu, S. X.; Kim, J.-T. *J. Assoc. Lab. Autom.* **2009**, *14*, 213–220.

(37) Voinova, M., V.; Rodahl, M.; Jonson, M.; Kasemo, B. *Phys. Scr.* **1999**, *59*, 391–396.

(38) Zhou, C.; Friedt, J.-M.; Angelova, A.; Choi, K.-H.; Laureyn, W.; Frederix, F.; Francis, L. A.; Campitelli, A.; Engelborghs, Y.; Borghs, G. *Langmuir* **2004**, *20*, 5870–5878.

(39) Voros, J. *Biophys. J.* **2004**, *87*, 553–561.

(40) Rodahl, M.; Hook, F.; Fredriksson, C.; Keller, C., A.; Krozer, A.; Brzezinski, P.; Voinovaa, M.; Kasemoa, B. *Faraday Discuss.* **1997**, *107*, 229–246.

(41) Paul, S.; Paul, D.; Basova, T.; Ray, A. K. *J. Phys. Chem. C* **2008**, *112*, 11822–11830.

(42) Leger, C.; Jones, A. K.; Albracht, S. P. J.; Armstrong, F. A. *J. Phys. Chem. B* **2002**, *106*, 13058–13063.

(43) Boubour, E.; Lennox, R. B. *Langmuir* **2000**, *16*, 7464–7470.

(44) Porter, M. D.; Bright, T. B.; Allara, D. L.; Chidseyi, C. E. D. *J. Am. Chem. Soc.* **1987**, *109*, 3559–3568.
(45) Sushko, M. L.; Shluger, A. L. *Adv. Funct. Mater.* **2008**, *18*, 2228–2236.
(46) Gozlan, N.; Tisch, U.; Haick, H. *J. Phys. Chem. C* **2008**, *112*, 12988–12992.
(47) Wang, L.; Rangger, G. M.; Romaner, L.; Heimel, G.; Bucko, T.; Ma, Z.; Li, Q.; Shuai, Z.; Zojer, E. *Adv. Funct. Mater.* **2009**, *19*, 3766–3775.
(48) Rissner, F.; Egger, D. A.; Romaner, L.; Heimel, G.; Zojer, E. *ASC Nano* **2010**, *4*, 6735–6746.
(49) Murphy, M. E.; Turley, S.; Kukimoto, M.; Nishiyama, M.; Horinouchi, S.; Sasaki, H.; Tanokura, M.; Adman, E. T. *Biochemistry* **1995**, *34*, 12107–12117.
(50) Impagliazzo, A.; Ubbink, M. *J. Am. Chem. Soc.* **2004**, *126*, 5658–5659.
(51) Kobayashi, K.; Tagawa, S.; Deligeer; Suzuki, S. *J. Biochem.* **1999**, *126*, 408–412.
(52) Suzuki, S.; Deligeer; Yamaguchi, K.; Kataoka, K.; Kobayashi, K.; Tagawa, S.; Kohzuma, T.; Shidara, S.; Iwasaki, H. *J. Biol. Inorg. Chem.* **1997**, *2*, 265–274.
(53) Fleming, B. D.; Praporski, S.; Bond, A. M.; Martin, L. L. *Langmuir* **2008**, *24*, 323–327.
(54) Saenger, W. *Annu. Rev. Biophys. Biophys. Chem.* **1987**, *16*, 93–114.
(55) Sauerbrey, G. *Z. Phys.* **1959**, *155*, 206–222.
(56) Dixon, M. C. *J. Biomol. Tech.* **2008**, *19*, 151–158.
(57) Janshoff, A.; Galla, H. J.; Steinem, C. *Angew. Chem., Int. Ed.* **2000**, *17*, 4004–4032.
(58) Höök, F.; Rodahl, M.; Brzezinski, P.; Kasemo, B. *Langmuir* **1998**, *14*, 729–734.
(59) Höök, F.; Kasemo, B. *Anal. Chem.* **2001**, *2001*, 5796–5804.